

# Study of $B^0 \rightarrow \rho^0 \rho^0$ decays, implications for the CKM angle $\phi_2$ and search for other four pion final states

I. Adachi,<sup>15</sup> K. Adamczyk,<sup>48</sup> H. Aihara,<sup>72</sup> K. Arinstein,<sup>3</sup> Y. Arita,<sup>41</sup> D. M. Asner,<sup>54</sup>  
T. Aso,<sup>76</sup> V. Aulchenko,<sup>3</sup> T. Aushev,<sup>27</sup> T. Aziz,<sup>67</sup> A. M. Bakich,<sup>66</sup> Y. Ban,<sup>56</sup> E. Barberio,<sup>40</sup>  
M. Barrett,<sup>14</sup> A. Bay,<sup>35</sup> I. Bedny,<sup>3</sup> M. Belhorn,<sup>6</sup> K. Belous,<sup>24</sup> V. Bhardwaj,<sup>44</sup> B. Bhuyan,<sup>19</sup>  
M. Bischofberger,<sup>44</sup> S. Blyth,<sup>46</sup> A. Bondar,<sup>3</sup> G. Bonvicini,<sup>78</sup> A. Bozek,<sup>48</sup> M. Bračko,<sup>38, 28</sup>  
J. Brodzicka,<sup>48</sup> O. Brovchenko,<sup>30</sup> T. E. Browder,<sup>14</sup> M.-C. Chang,<sup>7</sup> P. Chang,<sup>47</sup> Y. Chao,<sup>47</sup>  
V. Chekelian,<sup>39</sup> A. Chen,<sup>45</sup> K.-F. Chen,<sup>47</sup> P. Chen,<sup>47</sup> B. G. Cheon,<sup>13</sup> K. Chilikin,<sup>27</sup>  
R. Chistov,<sup>27</sup> I.-S. Cho,<sup>80</sup> K. Cho,<sup>31</sup> K.-S. Choi,<sup>80</sup> S.-K. Choi,<sup>12</sup> Y. Choi,<sup>65</sup> J. Crnkovic,<sup>18</sup>  
J. Dalseno,<sup>39, 68</sup> M. Danilov,<sup>27</sup> J. Dingfelder,<sup>2</sup> Z. Doležal,<sup>4</sup> Z. Drásal,<sup>4</sup> A. Drutskoy,<sup>27</sup>  
W. Dungel,<sup>23</sup> D. Dutta,<sup>19</sup> S. Eidelman,<sup>3</sup> D. Epifanov,<sup>3</sup> S. Esen,<sup>6</sup> J. E. Fast,<sup>54</sup> M. Feindt,<sup>30</sup>  
A. Frey,<sup>10</sup> M. Fujikawa,<sup>44</sup> V. Gaur,<sup>67</sup> N. Gabyshev,<sup>3</sup> A. Garmash,<sup>3</sup> Y. M. Goh,<sup>13</sup>  
B. Golob,<sup>36, 28</sup> M. Grosse Perdekamp,<sup>18, 60</sup> H. Guo,<sup>62</sup> J. Haba,<sup>15</sup> P. Hamer,<sup>10</sup> Y. L. Han,<sup>22</sup>  
K. Hara,<sup>15</sup> T. Hara,<sup>15</sup> Y. Hasegawa,<sup>64</sup> K. Hayasaka,<sup>42</sup> H. Hayashii,<sup>44</sup> D. Heffernan,<sup>53</sup>  
T. Higuchi,<sup>15</sup> Y. Horii,<sup>42</sup> Y. Hoshi,<sup>70</sup> K. Hoshina,<sup>75</sup> W.-S. Hou,<sup>47</sup> Y. B. Hsiung,<sup>47</sup>  
H. J. Hyun,<sup>34</sup> Y. Igarashi,<sup>15</sup> T. Iijima,<sup>42, 41</sup> M. Imamura,<sup>41</sup> K. Inami,<sup>41</sup> A. Ishikawa,<sup>71</sup>  
R. Itoh,<sup>15</sup> M. Iwabuchi,<sup>80</sup> M. Iwasaki,<sup>72</sup> Y. Iwasaki,<sup>15</sup> T. Iwashita,<sup>44</sup> S. Iwata,<sup>74</sup> I. Jaegle,<sup>14</sup>  
M. Jones,<sup>14</sup> T. Julius,<sup>40</sup> D. H. Kah,<sup>34</sup> H. Kakuno,<sup>74</sup> J. H. Kang,<sup>80</sup> P. Kapusta,<sup>48</sup>  
S. U. Kataoka,<sup>43</sup> N. Katayama,<sup>15</sup> H. Kawai,<sup>5</sup> T. Kawasaki,<sup>50</sup> H. Kichimi,<sup>15</sup> C. Kiesling,<sup>39</sup>  
B. H. Kim,<sup>63</sup> H. J. Kim,<sup>34</sup> H. O. Kim,<sup>34</sup> J. B. Kim,<sup>32</sup> J. H. Kim,<sup>31</sup> K. T. Kim,<sup>32</sup>  
M. J. Kim,<sup>34</sup> S. K. Kim,<sup>63</sup> Y. J. Kim,<sup>31</sup> K. Kinoshita,<sup>6</sup> J. Klucar,<sup>28</sup> B. R. Ko,<sup>32</sup>  
N. Kobayashi,<sup>73</sup> S. Koblitz,<sup>39</sup> P. Kodyš,<sup>4</sup> Y. Koga,<sup>41</sup> S. Korpar,<sup>38, 28</sup> R. T. Kouzes,<sup>54</sup>  
M. Kreps,<sup>30</sup> P. Križan,<sup>36, 28</sup> P. Krokovny,<sup>3</sup> B. Kronenbitter,<sup>30</sup> T. Kuhr,<sup>30</sup> R. Kumar,<sup>55</sup>  
T. Kumita,<sup>74</sup> E. Kurihara,<sup>5</sup> Y. Kuroki,<sup>53</sup> A. Kuzmin,<sup>3</sup> P. Kvasnička,<sup>4</sup> Y.-J. Kwon,<sup>80</sup>  
S.-H. Kyeong,<sup>80</sup> J. S. Lange,<sup>8</sup> M. J. Lee,<sup>63</sup> S.-H. Lee,<sup>32</sup> M. Leitgab,<sup>18, 60</sup> R. Leitner,<sup>4</sup>  
J. Li,<sup>63</sup> X. Li,<sup>63</sup> Y. Li,<sup>77</sup> J. Libby,<sup>20</sup> C.-L. Lim,<sup>80</sup> A. Limosani,<sup>40</sup> C. Liu,<sup>62</sup> Y. Liu,<sup>6</sup>  
Z. Q. Liu,<sup>22</sup> D. Liventsev,<sup>27</sup> R. Louvot,<sup>35</sup> J. MacNaughton,<sup>15</sup> D. Marlow,<sup>57</sup> D. Matvienko,<sup>3</sup>  
A. Matyja,<sup>48</sup> S. McOnie,<sup>66</sup> Y. Mikami,<sup>71</sup> K. Miyabayashi,<sup>44</sup> Y. Miyachi,<sup>79</sup> H. Miyata,<sup>50</sup>  
Y. Miyazaki,<sup>41</sup> R. Mizuk,<sup>27</sup> G. B. Mohanty,<sup>67</sup> D. Mohapatra,<sup>54</sup> A. Moll,<sup>39, 68</sup> T. Mori,<sup>41</sup>  
T. Müller,<sup>30</sup> N. Muramatsu,<sup>58</sup> R. Mussa,<sup>26</sup> T. Nagamine,<sup>71</sup> Y. Nagasaka,<sup>16</sup> Y. Nakahama,<sup>72</sup>  
I. Nakamura,<sup>15</sup> E. Nakano,<sup>52</sup> T. Nakano,<sup>59</sup> M. Nakao,<sup>15</sup> H. Nakayama,<sup>15</sup> H. Nakazawa,<sup>45</sup>  
Z. Natkaniec,<sup>48</sup> M. Nayak,<sup>20</sup> E. Nedelkovska,<sup>39</sup> K. Negishi,<sup>71</sup> K. Neichi,<sup>70</sup> S. Neubauer,<sup>30</sup>  
C. Ng,<sup>72</sup> M. Niiyama,<sup>33</sup> S. Nishida,<sup>15</sup> K. Nishimura,<sup>14</sup> O. Nitoh,<sup>75</sup> T. Nozaki,<sup>15</sup> A. Ogawa,<sup>60</sup>  
S. Ogawa,<sup>69</sup> T. Ohshima,<sup>41</sup> S. Okuno,<sup>29</sup> S. L. Olsen,<sup>63, 14</sup> Y. Onuki,<sup>72</sup> W. Ostrowicz,<sup>48</sup>  
H. Ozaki,<sup>15</sup> P. Pakhlov,<sup>27</sup> G. Pakhlova,<sup>27</sup> H. Palka,<sup>48</sup> E. Panzenböck,<sup>10, 44</sup> C. W. Park,<sup>65</sup>  
H. Park,<sup>34</sup> H. K. Park,<sup>34</sup> K. S. Park,<sup>65</sup> L. S. Peak,<sup>66</sup> T. K. Pedlar,<sup>37</sup> T. Peng,<sup>62</sup>  
R. Pestotnik,<sup>28</sup> M. Peters,<sup>14</sup> M. Petrič,<sup>28</sup> L. E. Piilonen,<sup>77</sup> A. Poluektov,<sup>3</sup> M. Prim,<sup>30</sup>  
K. Prothmann,<sup>39, 68</sup> B. Reisert,<sup>39</sup> M. Ritter,<sup>39</sup> M. Röhrken,<sup>30</sup> J. Rorie,<sup>14</sup> M. Rozanska,<sup>48</sup>  
S. Ryu,<sup>63</sup> H. Sahoo,<sup>14</sup> K. Sakai,<sup>15</sup> Y. Sakai,<sup>15</sup> S. Sandilya,<sup>67</sup> D. Santel,<sup>6</sup> L. Santelj,<sup>28</sup>  
T. Sanuki,<sup>71</sup> N. Sasao,<sup>33</sup> Y. Sato,<sup>71</sup> O. Schneider,<sup>35</sup> G. Schnell,<sup>1, 17</sup> P. Schönmeier,<sup>71</sup>  
C. Schwanda,<sup>23</sup> A. J. Schwartz,<sup>6</sup> B. Schwenker,<sup>10</sup> R. Seidl,<sup>60</sup> A. Sekiya,<sup>44</sup> K. Senyo,<sup>79</sup>

O. Seon,<sup>41</sup> M. E. Sevier,<sup>40</sup> L. Shang,<sup>22</sup> M. Shapkin,<sup>24</sup> V. Shebalin,<sup>3</sup> C. P. Shen,<sup>41</sup>  
T.-A. Shibata,<sup>73</sup> H. Shibuya,<sup>69</sup> S. Shinomiya,<sup>53</sup> J.-G. Shiu,<sup>47</sup> B. Shwartz,<sup>3</sup> A. Sibidanov,<sup>66</sup>  
F. Simon,<sup>39,68</sup> J. B. Singh,<sup>55</sup> R. Sinha,<sup>25</sup> P. Smerkol,<sup>28</sup> Y.-S. Sohn,<sup>80</sup> A. Sokolov,<sup>24</sup>  
E. Solovieva,<sup>27</sup> S. Stanić,<sup>51</sup> M. Starić,<sup>28</sup> J. Stypula,<sup>48</sup> S. Sugihara,<sup>72</sup> A. Sugiyama,<sup>61</sup>  
M. Sumihama,<sup>9</sup> K. Sumisawa,<sup>15</sup> T. Sumiyoshi,<sup>74</sup> K. Suzuki,<sup>41</sup> S. Suzuki,<sup>61</sup> S. Y. Suzuki,<sup>15</sup>  
H. Takeichi,<sup>41</sup> U. Tamponi,<sup>26</sup> M. Tanaka,<sup>15</sup> S. Tanaka,<sup>15</sup> K. Tanida,<sup>63</sup> N. Taniguchi,<sup>15</sup>  
G. Tatishvili,<sup>54</sup> G. N. Taylor,<sup>40</sup> Y. Teramoto,<sup>52</sup> F. Thorne,<sup>23</sup> I. Tikhomirov,<sup>27</sup> K. Trabelsi,<sup>15</sup>  
Y. F. Tse,<sup>40</sup> T. Tsuboyama,<sup>15</sup> M. Uchida,<sup>73</sup> T. Uchida,<sup>15</sup> Y. Uchida,<sup>11</sup> S. Uehara,<sup>15</sup>  
K. Ueno,<sup>47</sup> T. Uglov,<sup>27</sup> Y. Unno,<sup>13</sup> S. Uno,<sup>15</sup> P. Urquijo,<sup>2</sup> Y. Ushiroda,<sup>15</sup> Y. Usov,<sup>3</sup>  
S. E. Vahsen,<sup>14</sup> P. Vanhoefer,<sup>39</sup> C. Van Hulse,<sup>1</sup> G. Varner,<sup>14</sup> K. E. Varvell,<sup>66</sup> K. Vervink,<sup>35</sup>  
A. Vinokurova,<sup>3</sup> V. Vorobyev,<sup>3</sup> A. Vossen,<sup>21</sup> C. H. Wang,<sup>46</sup> J. Wang,<sup>56</sup> M.-Z. Wang,<sup>47</sup>  
P. Wang,<sup>22</sup> X. L. Wang,<sup>22</sup> M. Watanabe,<sup>50</sup> Y. Watanabe,<sup>29</sup> R. Wedd,<sup>40</sup> E. White,<sup>6</sup>  
J. Wicht,<sup>15</sup> L. Widhalm,<sup>23</sup> J. Wiechczynski,<sup>48</sup> K. M. Williams,<sup>77</sup> E. Won,<sup>32</sup> B. D. Yabsley,<sup>66</sup>  
H. Yamamoto,<sup>71</sup> J. Yamaoka,<sup>14</sup> Y. Yamashita,<sup>49</sup> M. Yamauchi,<sup>15</sup> C. Z. Yuan,<sup>22</sup> Y. Yusa,<sup>50</sup>  
D. Zander,<sup>30</sup> C. C. Zhang,<sup>22</sup> L. M. Zhang,<sup>62</sup> Z. P. Zhang,<sup>62</sup> L. Zhao,<sup>62</sup> V. Zhilich,<sup>3</sup>  
P. Zhou,<sup>78</sup> V. Zhulanov,<sup>3</sup> T. Zivko,<sup>28</sup> A. Zupanc,<sup>30</sup> N. Zwahlen,<sup>35</sup> and O. Zyukova<sup>3</sup>

(The Belle Collaboration)

<sup>1</sup>*University of the Basque Country UPV/EHU, Bilbao*

<sup>2</sup>*University of Bonn, Bonn*

<sup>3</sup>*Budker Institute of Nuclear Physics SB RAS and  
Novosibirsk State University, Novosibirsk 630090*

<sup>4</sup>*Faculty of Mathematics and Physics, Charles University, Prague*

<sup>5</sup>*Chiba University, Chiba*

<sup>6</sup>*University of Cincinnati, Cincinnati, Ohio 45221*

<sup>7</sup>*Department of Physics, Fu Jen Catholic University, Taipei*

<sup>8</sup>*Justus-Liebig-Universität Gießen, Gießen*

<sup>9</sup>*Gifu University, Gifu*

<sup>10</sup>*II. Physikalisches Institut, Georg-August-Universität Göttingen, Göttingen*

<sup>11</sup>*The Graduate University for Advanced Studies, Hayama*

<sup>12</sup>*Gyeongsang National University, Chinju*

<sup>13</sup>*Hanyang University, Seoul*

<sup>14</sup>*University of Hawaii, Honolulu, Hawaii 96822*

<sup>15</sup>*High Energy Accelerator Research Organization (KEK), Tsukuba*

<sup>16</sup>*Hiroshima Institute of Technology, Hiroshima*

<sup>17</sup>*IKERBASQUE, Bilbao*

<sup>18</sup>*University of Illinois at Urbana-Champaign, Urbana, Illinois 61801*

<sup>19</sup>*Indian Institute of Technology Guwahati, Guwahati*

<sup>20</sup>*Indian Institute of Technology Madras, Madras*

<sup>21</sup>*Indiana University, Bloomington, Indiana 47408*

<sup>22</sup>*Institute of High Energy Physics,*

*Chinese Academy of Sciences, Beijing*

<sup>23</sup>*Institute of High Energy Physics, Vienna*

<sup>24</sup>*Institute of High Energy Physics, Protvino*

<sup>25</sup>*Institute of Mathematical Sciences, Chennai*

<sup>26</sup>*INFN - Sezione di Torino, Torino*

- <sup>27</sup>*Institute for Theoretical and Experimental Physics, Moscow*  
<sup>28</sup>*J. Stefan Institute, Ljubljana*  
<sup>29</sup>*Kanagawa University, Yokohama*  
<sup>30</sup>*Institut für Experimentelle Kernphysik,  
Karlsruher Institut für Technologie, Karlsruhe*  
<sup>31</sup>*Korea Institute of Science and Technology Information, Daejeon*  
<sup>32</sup>*Korea University, Seoul*  
<sup>33</sup>*Kyoto University, Kyoto*  
<sup>34</sup>*Kyungpook National University, Taegu*  
<sup>35</sup>*École Polytechnique Fédérale de Lausanne (EPFL), Lausanne*  
<sup>36</sup>*Faculty of Mathematics and Physics, University of Ljubljana, Ljubljana*  
<sup>37</sup>*Luther College, Decorah, Iowa 52101*  
<sup>38</sup>*University of Maribor, Maribor*  
<sup>39</sup>*Max-Planck-Institut für Physik, München*  
<sup>40</sup>*University of Melbourne, School of Physics, Victoria 3010*  
<sup>41</sup>*Graduate School of Science, Nagoya University, Nagoya*  
<sup>42</sup>*Kobayashi-Maskawa Institute, Nagoya University, Nagoya*  
<sup>43</sup>*Nara University of Education, Nara*  
<sup>44</sup>*Nara Women's University, Nara*  
<sup>45</sup>*National Central University, Chung-li*  
<sup>46</sup>*National United University, Miao Li*  
<sup>47</sup>*Department of Physics, National Taiwan University, Taipei*  
<sup>48</sup>*H. Niewodniczanski Institute of Nuclear Physics, Krakow*  
<sup>49</sup>*Nippon Dental University, Niigata*  
<sup>50</sup>*Niigata University, Niigata*  
<sup>51</sup>*University of Nova Gorica, Nova Gorica*  
<sup>52</sup>*Osaka City University, Osaka*  
<sup>53</sup>*Osaka University, Osaka*  
<sup>54</sup>*Pacific Northwest National Laboratory, Richland, Washington 99352*  
<sup>55</sup>*Panjab University, Chandigarh*  
<sup>56</sup>*Peking University, Beijing*  
<sup>57</sup>*Princeton University, Princeton, New Jersey 08544*  
<sup>58</sup>*Research Center for Electron Photon Science, Tohoku University, Sendai*  
<sup>59</sup>*Research Center for Nuclear Physics, Osaka University, Osaka*  
<sup>60</sup>*RIKEN BNL Research Center, Upton, New York 11973*  
<sup>61</sup>*Saga University, Saga*  
<sup>62</sup>*University of Science and Technology of China, Hefei*  
<sup>63</sup>*Seoul National University, Seoul*  
<sup>64</sup>*Shinshu University, Nagano*  
<sup>65</sup>*Sungkyunkwan University, Suwon*  
<sup>66</sup>*School of Physics, University of Sydney, NSW 2006*  
<sup>67</sup>*Tata Institute of Fundamental Research, Mumbai*  
<sup>68</sup>*Excellence Cluster Universe, Technische Universität München, Garching*  
<sup>69</sup>*Toho University, Funabashi*  
<sup>70</sup>*Tohoku Gakuin University, Tagajo*  
<sup>71</sup>*Tohoku University, Sendai*  
<sup>72</sup>*Department of Physics, University of Tokyo, Tokyo*

<sup>73</sup>*Tokyo Institute of Technology, Tokyo*

<sup>74</sup>*Tokyo Metropolitan University, Tokyo*

<sup>75</sup>*Tokyo University of Agriculture and Technology, Tokyo*

<sup>76</sup>*Toyama National College of Maritime Technology, Toyama*

<sup>77</sup>*CNP, Virginia Polytechnic Institute and State University, Blacksburg, Virginia 24061*

<sup>78</sup>*Wayne State University, Detroit, Michigan 48202*

<sup>79</sup>*Yamagata University, Yamagata*

<sup>80</sup>*Yonsei University, Seoul*

## Abstract

We present a study of the branching fraction of the decay  $B^0 \rightarrow \rho^0 \rho^0$  and the fraction of longitudinally polarized  $\rho^0$  mesons in this decay. The results are obtained from the final data sample containing  $772 \times 10^6$   $B\bar{B}$  pairs collected at the  $\Upsilon(4S)$  resonance with the Belle detector at the KEKB asymmetric-energy  $e^+e^-$  collider. We find  $166 \pm 59$   $B^0 \rightarrow \rho^0 \rho^0$  events, corresponding to a branching fraction of  $\mathcal{B}(B^0 \rightarrow \rho^0 \rho^0) = (1.02 \pm 0.30 \text{ (stat)} \pm 0.22 \text{ (syst)}) \times 10^{-6}$  with a longitudinally polarization fraction  $f_L = 0.21^{+0.18}_{-0.22} \text{ (stat)} \pm 0.11 \text{ (syst)}$ . The branching fraction's upper limit is

$$\mathcal{B}(B^0 \rightarrow \rho^0 \rho^0) < 1.5 \times 10^{-6}$$

at 90% confidence level. We use the longitudinal polarization fraction to determine the Cabibbo-Kobayashi-Maskawa matrix angle  $\phi_2 = (91.0 \pm 7.2)^\circ$  through an isospin analysis in the  $B \rightarrow \rho\rho$  system. We furthermore obtain

$$\mathcal{B}(B^0 \rightarrow f_0 \rho^0) \times \mathcal{B}(f_0 \rightarrow \pi^+ \pi^-) = (0.86 \pm 0.27 \text{ (stat)} \pm 0.15 \text{ (syst)}) \times 10^{-6},$$

corresponding to  $149 \pm 49$   $B^0 \rightarrow f_0 \rho^0$  events with a significance of 3.0 standard deviations and upper limits at 90% confidence level on the (product) branching fractions for possible decays with the same final state,

$$\begin{aligned} \mathcal{B}(B^0 \rightarrow \pi^+ \pi^- \pi^+ \pi^-) &< 11.7 \times 10^{-6}, \\ \mathcal{B}(B^0 \rightarrow \rho^0 \pi^+ \pi^-) &< 12.2 \times 10^{-6}, \\ \mathcal{B}(B^0 \rightarrow f_0 \pi^+ \pi^-) \times \mathcal{B}(f_0 \rightarrow \pi^+ \pi^-) &< 3.1 \times 10^{-6} \text{ and} \\ \mathcal{B}(B^0 \rightarrow f_0 f_0) \times \mathcal{B}(f_0 \rightarrow \pi^+ \pi^-)^2 &< 0.2 \times 10^{-6}. \end{aligned}$$

PACS numbers: 11.30.Er, 12.15.Hh, 13.25.Hw

## I. INTRODUCTION

$CP$  violation in the standard model (SM) is due to an irreducible complex phase in the Cabibbo-Kobayashi-Maskawa (CKM) quark-mixing matrix [1, 2]. Mixing-induced  $CP$  violation in the  $B$  sector has been clearly observed by the Belle [3, 4] and BaBar [5, 6] collaborations in the  $b \rightarrow c\bar{c}s$  induced decay  $B^0 \rightarrow J/\psi K_S^0$ , while many other modes provide additional information on  $CP$  violating parameters.

Decays that proceed predominantly through the  $b \rightarrow u\bar{u}d$  transition are sensitive to one of the angles of the unitarity triangle,  $\phi_2$  (or  $\alpha$ )  $\equiv \arg[(-V_{td}V_{tb}^*)/(V_{ud}V_{ub}^*)]$ . The Belle and BaBar collaborations have reported time-dependent  $CP$  asymmetries in these modes that include decays such as  $B^0 \rightarrow \pi^+\pi^-$  [7, 8],  $\rho^\pm\pi^\mp$  [9, 10],  $\rho^+\rho^-$  [11, 12] and  $a_1^\pm\pi^\mp$  [13–15]. A feature common to these measurements is that possible loop contributions, in addition to the leading order tree amplitude, can shift the measured angle to  $\phi_2^{\text{eff}} \equiv \phi_2 + \Delta\phi_2$ . Fortunately, this inconvenience can be overcome with bounds on  $\Delta\phi_2$  determined using either an isospin analysis [16] or  $SU(3)$  flavor symmetry [17].

This analysis is concerned with the branching fraction of  $B^0 \rightarrow \rho^0\rho^0$  decays, shown in Fig. 1, the fraction of longitudinal polarization in these decays and decays into four charged pion final states as the  $\rho^0$  decays dominantly into two charged pions.

Since the dominant tree process is color-suppressed,  $B^0 \rightarrow \rho^0\rho^0$  is expected to be rarer than its isospin partners, making the isospin analysis less ambiguous. The vector state  $\rho^0\rho^0$  is not a pure  $CP$  eigenstate, but rather a superposition of  $CP$ -even and -odd states, or three helicity amplitudes, with only the longitudinal one being a pure  $CP$  eigenstate. In general, the different helicity amplitudes can be separated through an angular analysis. Here, we use the helicity basis where the angle  $\theta_{Hk}|_{k=1,2}$ , defined as the angle between the  $\pi^+$ 's and the  $B$ 's flight directions in the rest frame of the  $k^{\text{th}}$   $\rho^0$  (Fig. 2), can be used to separate longitudinally ( $CP$ -even) from transversely ( $CP$ -even and -odd) polarized  $\rho^0$  mesons. The angular distribution is given by

$$\frac{d^2\Gamma}{\Gamma d\cos\theta_{H1}d\cos\theta_{H2}} = \frac{9}{4} \left[ \frac{1}{4}(1 - f_L) \sin^2\theta_{H1} \sin^2\theta_{H2} + f_L \cos^2\theta_{H1} \cos^2\theta_{H2} \right] \quad (1)$$

where  $f_L = |A_0|^2 / \sum |A_i|^2$  is the fraction of longitudinal polarization;  $A_0$ ,  $A_{+1}$  and  $A_{-1}$  are the helicity amplitudes.

The SM, using perturbative QCD (pQCD) [18] or QCD factorization [19, 20], predicts the  $B^0 \rightarrow \rho^0\rho^0$  branching fraction to be  $\sim 1 \times 10^{-6}$ . Analogous to the decay of a  $B^0$  meson

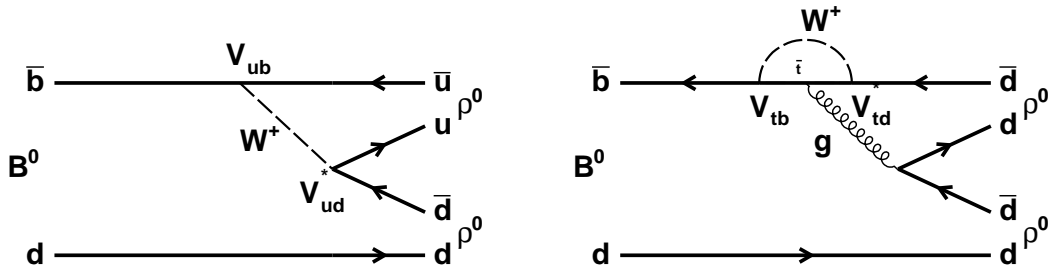


FIG. 1: Leading-order tree (left) and penguin (right) diagrams for the decay  $B^0 \rightarrow \rho^0\rho^0$ .

into two charged  $\rho$  mesons, the decay  $B^0 \rightarrow \rho^0 \rho^0$  is expected to be predominantly longitudinally polarized. However, color-suppressed  $B$  meson decays into two vector particles are especially difficult to predict. Hence, this analysis provides an excellent test of the theoretical assumptions used in these calculations and improves our understanding of the helicity structure of the weak interaction.

Using a sample containing  $657 \times 10^6$   $B\bar{B}$  pairs and assuming pure longitudinal polarization, the previous Belle analysis set an upper limit on the branching fraction of  $B^0 \rightarrow \rho^0 \rho^0$  decays;  $\mathcal{B}(B^0 \rightarrow \rho^0 \rho^0) < 1.0 \times 10^{-6}$  at 90% confidence level (CL) [21]. The BaBar collaboration has performed a study of  $B^0 \rightarrow \rho^0 \rho^0$  decays with  $465 \times 10^6$   $B\bar{B}$  pairs and found a branching fraction  $\mathcal{B}(B^0 \rightarrow \rho^0 \rho^0) = (0.92 \pm 0.32(\text{stat}) \pm 0.14(\text{syst})) \times 10^{-6}$  and a longitudinal polarization fraction of  $f_L = 0.75^{+0.11}_{-0.14}(\text{stat}) \pm 0.04(\text{syst})$  [22].

In Sec. II, we briefly describe the data set and the Belle detector. The event selection and the model used for the branching fraction measurement are described in sections III and IV, respectively. Next, the fit result is presented in Sec. V, followed by validity checks in Sec. VI, where the significance of the fit result is discussed as well. The systematic uncertainties are given in Sec. VII and a constraint of the CKM phase  $\phi_2$  is presented in Sec. VIII, followed by our conclusion.

## II. DATA SET AND BELLE DETECTOR

This measurement is based on the final data sample containing  $772 \times 10^6$   $B\bar{B}$  pairs collected with the Belle detector at the KEKB asymmetric-energy  $e^+e^-$  (3.5 on 8 GeV) collider [23]. At the  $\Upsilon(4S)$  resonance ( $\sqrt{s} = 10.58$  GeV), the Lorentz boost of the produced  $B\bar{B}$  pairs was  $\beta\gamma = 0.425$  along the  $z$  direction, which is opposite the positron beam direction.

The Belle detector is a large-solid-angle magnetic spectrometer that consists of a silicon vertex detector (SVD), a 50-layer central drift chamber (CDC), an array of aerogel threshold Cherenkov counters (ACC), a barrel-like arrangement of time-of-flight scintillation counters (TOF), and an electromagnetic calorimeter comprising of CsI(Tl) crystals (ECL) located inside a superconducting solenoid coil that provides a 1.5 T magnetic field. An iron flux-return located outside of the coil is instrumented to detect  $K_L^0$  mesons and to identify muons (KLM). The detector is described in detail elsewhere [24].

Two inner detector configurations were used. A 2.0 cm radius beampipe and a 3-layer silicon vertex detector (SVD1) was used for the first sample of  $152 \times 10^6$   $B\bar{B}$  pairs, while a 1.5 cm radius beampipe, a 4-layer silicon detector (SVD2) and a small-cell inner drift

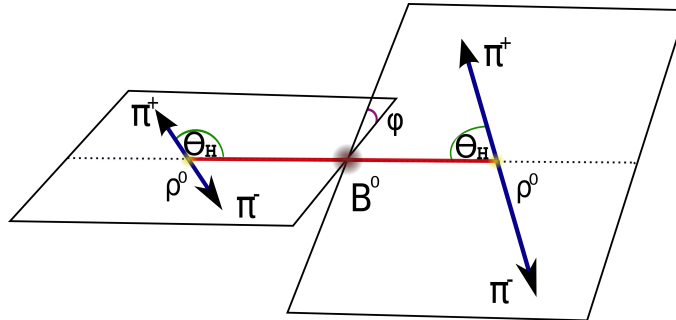


FIG. 2: Definition of the helicity angles  $\theta_{Hk}$  for each  $\rho$ , identified by index  $k = 1, 2$ .



TABLE I: Summary of peaking background vetoes. A muon mass hypotheses has been applied to specific tracks for the  $J/\psi$  channel. Here,  $\pi_1^+\pi_2^-$  forms the first  $\rho^0$  candidate and  $\pi_3^+\pi_4^-$  the other.  $X$  represents any intermediate state or track combination that leads to a 4-body final state.

Regions vetoed	Modes vetoed
$1.85 \text{ GeV}/c^2 < m(\pi^+\pi^-) < 1.89 \text{ GeV}/c^2$	$B \rightarrow D^0[\pi^+\pi^-]X$
$1.85 \text{ GeV}/c^2 < m(\pi_1^+\pi_2^-\pi_3^+) < 1.89 \text{ GeV}/c^2$	$B \rightarrow D^+[\pi^+\pi^-\pi^+]X$
$1.85 \text{ GeV}/c^2 < m(\pi_2^-\pi_3^+\pi_4^-) < 1.89 \text{ GeV}/c^2$	$B \rightarrow D^-[\pi^-\pi^+\pi^-]X$
$1.95 \text{ GeV}/c^2 < m(\pi_1^+\pi_2^-\pi_3^+) < 1.99 \text{ GeV}/c^2$	$B \rightarrow D_s^+[\pi^+\pi^-\pi^+]X$
$1.95 \text{ GeV}/c^2 < m(\pi_2^-\pi_3^+\pi_4^-) < 1.99 \text{ GeV}/c^2$	$B \rightarrow D_s^-[\pi^-\pi^+\pi^-]X$
$3.06 \text{ GeV}/c^2 < m(\mu^+\mu^-) < 3.14 \text{ GeV}/c^2$	$B \rightarrow J/\psi[\mu^+\mu^-]X$
$0.478 \text{ GeV}/c^2 < m(\pi_2\pi_3) < 0.512 \text{ GeV}/c^2$	$B \rightarrow K_S^0[\pi^+\pi^-]X$

chamber were used to record the remaining  $620 \times 10^6 B\bar{B}$  pairs [25]. We use a GEANT-based Monte Carlo (MC) simulation to model the response of the detector and determine its acceptance [26].

### III. EVENT SELECTION

We reconstruct  $B^0 \rightarrow \rho^0\rho^0$  where  $\rho^0 \rightarrow \pi^+\pi^-$ . Charged tracks have to fulfill loose requirements on the distance of closest approach to the interaction point (IP) of  $|dz| < 5.0$  cm and  $dr < 0.5$  cm along and perpendicular to the  $z$  axis, respectively. With information obtained from the CDC, ACC and TOF, particle identification (PID) is determined with the likelihood ratio  $\mathcal{L}_{i/j} \equiv \mathcal{L}_i/(\mathcal{L}_i + \mathcal{L}_j)$ , where  $\mathcal{L}_i$  ( $\mathcal{L}_j$ ) is the likelihood that the particle is of type  $i$  ( $j$ ). We require  $\mathcal{L}_{K/\pi} < 0.4$ , which retains 90% of all pions but only 10% of kaons. In addition, we place vetoes on particles consistent with the electron or proton hypotheses. SVD requirements of two  $z$  hits and one  $r - \phi$  hit [27] are imposed on the charged tracks, to permit a subsequent measurement of the  $CP$  asymmetries.

Intermediate dipion states are reconstructed above the  $K_S^0$  region with an invariant mass  $0.52 \text{ GeV}/c^2 < m(\pi^+\pi^-) < 1.15 \text{ GeV}/c^2$  straddling the broad  $\rho^0(770)$  resonance [28]. This range retains 93% of all  $\rho^0$ . Upon combination of two dipion states, a  $B$  candidate is formed. All remaining particles are associated with the accompanying  $B$  meson in the event, referred to as  $B_{\text{Tag}}^0$ .

Reconstructed  $B$  candidates are described with two kinematic variables: the beam-energy-constrained mass  $M_{\text{bc}} \equiv \sqrt{(E_{\text{beam}}^{\text{CMS}}/c^2)^2 - (p_B^{\text{CMS}}/c)^2}$ , and the energy difference  $\Delta E \equiv E_B^{\text{CMS}} - E_{\text{beam}}^{\text{CMS}}$ , where  $E_{\text{beam}}^{\text{CMS}}$  is the beam energy and  $E_B^{\text{CMS}}$  ( $p_B^{\text{CMS}}$ ) is the energy (momentum) of the  $B$  meson, evaluated in the center-of-mass system (CMS). The  $B$  candidates that satisfy  $M_{\text{bc}} > 5.27 \text{ GeV}/c^2$  and  $|\Delta E| < 0.1 \text{ GeV}$  are selected for further analysis.

To reduce peaking background coming from charm ( $b \rightarrow c$ ) decays of the  $B$  meson with a similar final-state topology such as  $B^0 \rightarrow D^-[\pi^-\pi^+\pi^-]\pi^+$  or backgrounds due to particle mis-identification, we place vetoes on various combinations of the four charged tracks forming our  $B^0$  candidate, as summarized in Table I. The total efficiency loss due to these vetoes is 4.4%. The dominant background contribution comes from continuum ( $e^+e^- \rightarrow q\bar{q}$ , where  $q = u, d, s, c$ ) events. We can use their jet-like topology to separate them from the more spherical  $B\bar{B}$  decays using a Fisher discriminant  $\mathcal{F}_{S/B}$  constructed from the following seven

variables:

- $L_2^{c,n} \equiv \sum_{c,n} p_{c,n}^{\text{CMS}} \cos^2 \theta_{p_{c,n}^{\text{CMS}}, \text{TB}}$ , where the sum of the CMS momenta runs over the charged tracks ( $c$ ) and neutral clusters ( $n$ ) on the tag side; the angle is between the particle direction and  $B$  thrust direction.
- $\cos \theta_{\text{TB}, \text{TO}}$ , where the angle is between the  $B$  thrust direction and the thrust of the tag side.
- $\cos \theta_{B,z}$ , where the angle is between the  $B$  flight direction and the  $z$  direction.
- $h_k^{so} \equiv \sum_{i,j_k} |\vec{p}_i| |\vec{p}_{j_k}| |P_2(\cos(\theta_{ij_k}))|$ , where  $\vec{p}_i$  is the CMS momentum of the  $i^{\text{th}}$  track from the signal side ( $s$ ),  $\vec{p}_{j_k}$  is the CMS momentum of the  $j_k^{\text{th}}$  particle from the other side ( $o$ ),  $\theta_{ij_k}$  is the angle between particle  $i$  and  $j_k$  and  $P_2$  is the second order Legendre polynomial. For the other side, we distinguish three cases using index  $k = 0, 1$  and  $2$ , for charged tracks, neutral particles and missing energy (treated as a particle), respectively,

which are shown in Fig. 3. The  $B\bar{B}$  and  $q\bar{q}$  training sample is taken from signal MC

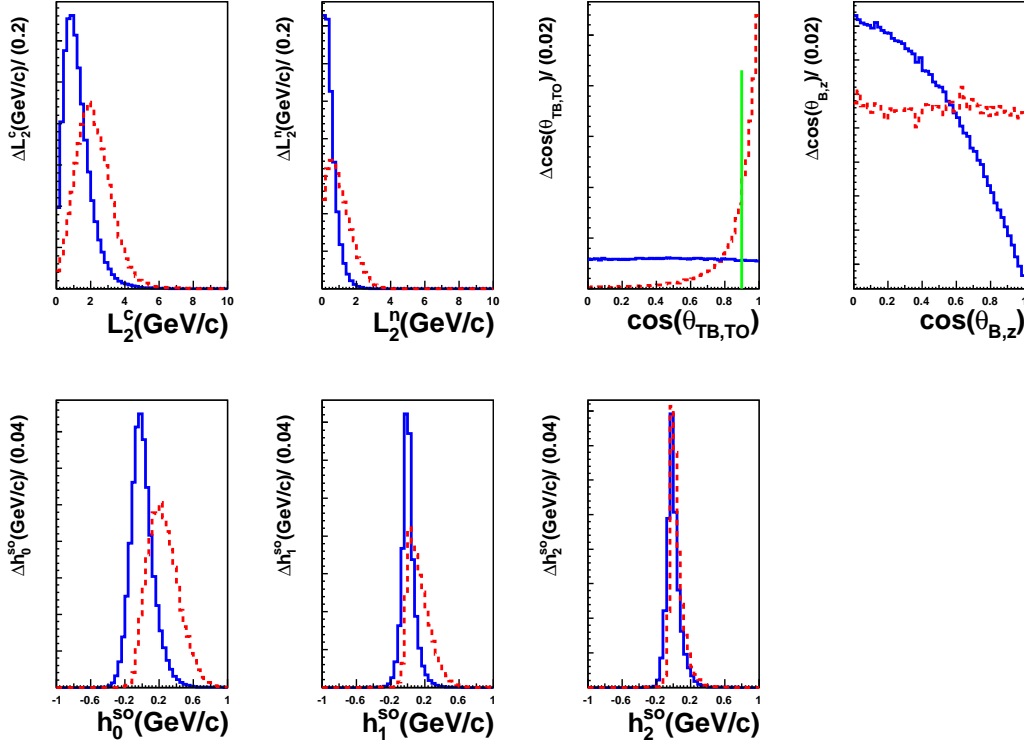


FIG. 3: (color online) Simulated (MC) and off-resonance data distributions for the quantities used to construct the Fisher discriminant  $\mathcal{F}_{S/B}$ , normalized to have the same area. The solid (blue) histograms shows the distribution for  $B\bar{B}$ , while the dashed (red) histograms show distributions for  $(q\bar{q})$  events from data taken below the  $\Upsilon(4S)$  resonance. The vertical line implies the cut  $\cos \theta_{\text{TB}, \text{TO}} < 0.9$ .

and from data taken below the  $\Upsilon(4S)$  resonance, respectively, and a loose requirement of



TABLE II: The reconstruction efficiencies ( $\epsilon$ ) of the signal for the four pion final states calculated from Monte Carlo, where the errors are statistical. For  $B^0 \rightarrow \rho^0 \rho^0$ , we use the  $f_L$  value obtained from the fit to data.

$\epsilon$ (mode)	SVD1 (%)	SVD2 (%)
$B^0 \rightarrow \rho^0 \rho^0$	$22.38 \pm 0.05$	$25.38 \pm 0.06$
$B^0 \rightarrow f_0 f_0$	$24.73 \pm 0.06$	$28.11 \pm 0.07$
$B^0 \rightarrow f_0 \rho^0$	$23.42 \pm 0.05$	$26.96 \pm 0.07$
$B^0 \rightarrow f_0 \pi^+ \pi^-$	$2.82 \pm 0.02$	$3.16 \pm 0.02$
$B^0 \rightarrow \rho^0 \pi^+ \pi^-$	$2.64 \pm 0.02$	$3.02 \pm 0.02$
$B^0 \rightarrow \pi^+ \pi^- \pi^+ \pi^-$	$0.98 \pm 0.01$	$1.09 \pm 0.01$

$\cos \theta_{\text{TB,TO}} < 0.9$  is placed that retains 90% signal while rejecting 50% of the continuum background. The Fisher discriminant is also required to satisfy  $-3 < \mathcal{F}_{S/B} < 2$ , this, together with the previous mentioned requirements of  $|\Delta E| < 0.1$  GeV,  $M_{\text{bc}} > 5.27$  GeV/ $c^2$  and  $0.52$  GeV/ $c^2 < m(\pi^+ \pi^-) < 1.15$  GeV/ $c^2$ , defines the fit region.

On average, 1.06  $B$  candidates are reconstructed per signal event. Selecting the best  $B$  candidate having  $M_{\text{bc}}$  nearest the nominal  $B$  meson mass [28], the correct  $B$  is chosen in 75% of all events with multiple candidates. If both possible dipion combinations of the four pions fall within the fit region, the dipion with the largest momentum difference between its pions is chosen. Since our selection criteria biases the  $M_{\text{bc}}$  distributions, we do not use this variable in the fit to data. The fraction of mis-reconstructed signal events is found to be 10%.

We also perform a vertex fit and employ the flavor tagging routine described in Ref. [29]. The tagging information is represented by two parameters, the  $B_{\text{Tag}}^0$  flavor  $q = \pm 1$ , and the tagging quality  $r$ . The parameter  $r$  is an event-by-event, MC determined flavor-tagging dilution factor that ranges from  $r = 0$  for no flavor discrimination to  $r = 1$  for unambiguous flavor assignment. The data is divided into 7  $r$ -bins, denoted as  $l$ .

We study backgrounds coming from  $b \rightarrow u\bar{u}d$  channels with the same final state as signal, namely  $B^0 \rightarrow a_1^\pm \pi^\mp$ ,  $a_2^\pm \pi^\mp$ ,  $b_1^\pm \pi^\mp$ ,  $f_0(980)\rho^0$ ,  $f_0(980)f_0(980)$ ,  $\rho^0 \pi^+ \pi^-$ ,  $f_0(980)\pi^+ \pi^-$ ,  $\pi^+ \pi^- \pi^+ \pi^-$ . The detection efficiencies  $\epsilon$  of the considered four charged pion final states after applying all mentioned selection criteria are listed in Table II.

We also determine correction factors to the efficiency that account for the differences between data and MC as calculated by independent internal studies at Belle. The correction factors  $\eta$  arising from particle identification criteria are listed in Table III.

Last, we remove an artificial asymmetry arising mainly from momentum ordering in the reconstruction by interchanging the two  $\rho^0$  candidates for odd event numbers.

#### IV. EVENT MODEL

The branching fraction is extracted from a six-dimensional extended unbinned maximum likelihood fit to  $\Delta E$ ,  $\mathcal{F}_{S/B}$ ,  $M_1$ ,  $M_2$ ,  $H_1$  and  $H_2$  in the  $l^{\text{th}}$   $r$ -bin and SVD configuration  $s$  where  $M_k$  and  $H_k$  represents the invariant dipion mass  $m_{\pi^+ \pi^-}$  and helicity parameter  $\cos \theta_H$ , respectively, of the  $\rho^0$  candidate, identified by index  $k = 1, 2$ . If linear correla-

TABLE III: Correction factors ( $\eta$ ) accounting for the difference between data and MC in particle identification. The errors are statistical. For  $B^0 \rightarrow \rho^0 \rho^0$ , we use the  $f_L$  value obtained from the fit to data.

$\eta$ (mode)	SVD1	SVD2
$B^0 \rightarrow \rho^0 \rho^0$	$0.84 \pm 0.02$	$0.85 \pm 0.03$
$B^0 \rightarrow f_0 f_0$	$0.84 \pm 0.02$	$0.85 \pm 0.03$
$B^0 \rightarrow f_0 \rho^0$	$0.84 \pm 0.03$	$0.86 \pm 0.03$
$B^0 \rightarrow f_0 \pi^+ \pi^-$	$0.84 \pm 0.02$	$0.85 \pm 0.03$
$B^0 \rightarrow \rho^0 \pi^+ \pi^-$	$0.84 \pm 0.02$	$0.85 \pm 0.03$
$B^0 \rightarrow \pi^+ \pi^- \pi^+ \pi^-$	$0.84 \pm 0.02$	$0.85 \pm 0.03$

tions between fit variables do not cause a noteworthy bias, the probability density function (PDF) for each event  $i$ , is taken as the product of individual PDFs for each variable  $\mathcal{P}(\Delta E^i, \mathcal{F}_{S/B}^i, M_1^i, M_2^i, H_1^i, H_2^i) = \mathcal{P}(\Delta E^i) \times \mathcal{P}(\mathcal{F}_{S/B}^i) \times \mathcal{P}(M_1^i) \times \mathcal{P}(M_2^i) \times \mathcal{P}(H_1^i) \times \mathcal{P}(H_2^i)$ ; otherwise, correlations between the fit variables are taken into account as described later on. We consider 17 components in the event model, where most resonances are described by a relativistic Breit-Wigner

$$BW(x, m_0, \Gamma) \equiv \frac{m_0 \Gamma(x)}{(x^2 - m_0^2)^2 + m_0^2 \Gamma^2(x)}, \quad (2)$$

with a mass-dependent width

$$\Gamma(m) = \Gamma_{\rho^0} \left( \frac{p_{\pi^+ \pi^-}}{p_{\rho^0}} \right)^3 \left( \frac{m_{\pi^+ \pi^-}}{m_{\rho^0}} \right) B_1(p_{\pi^+ \pi^-}, p_{\rho^0}); \quad (3)$$

$\Gamma_{\rho^0}$  is the nominal width of the  $\rho^0$ ,  $p_{\pi^+ \pi^-}$  ( $m_{\pi^+ \pi^-}$ ) the momentum (invariant mass) of a pion pair and  $p_{\rho^0}$  ( $m_{\rho^0}$ ) the momentum (invariant mass) of the nominal  $\rho^0$  coming from  $B^0 \rightarrow \rho^0 \rho^0$  decays.  $B_1$  is a Blatt-Weisskopf form factor as described in Ref. [28].

The signal model shape is determined from correctly reconstructed signal MC events. The PDF for  $\Delta E$  for all four pion final states is taken to be a sum of two asymmetric-width (bifurcated) Gaussians incorporating calibration factors that correct for the difference between data and MC. These factors calibrate the mean and width of the core bifurcated Gaussian. They are determined from a large statistics control sample  $B^0 \rightarrow D^- [K^+ \pi^- \pi^-] \pi^+$  and are used for all four pion final states. Similarly, the parameters describing the signal's core Gaussian are made common among all four charged pion final states. The PDF for  $\mathcal{F}_{S/B}$ , here and throughout this analysis for all components  $j$ , is the sum of two bifurcated Gaussians in each  $r$ -bin, incorporating calibration factors that correct for the difference between data and MC for all  $B\bar{B}$  components as their shapes are determined from MC. The shape for all other  $B\bar{B}$  components is fixed from the signal model except for the mean and width of their core distribution. The distribution in the  $M_1$ - $M_2$  plane is modelled with a two-dimensional (2D) efficiency-corrected product of two relativistic Breit-Wigner functions; the distribution in the  $H_1$ - $H_2$  plane is described by Eq. 1, corrected by a 2D efficiency histogram obtained from fully simulated signal MC.

The mis-reconstructed model shape is determined from incorrectly reconstructed signal MC events and its PDF is a histogram for all fit variables, smoothed if applicable.

The continuum model shape was studied with data taken below the  $\Upsilon(4S)$  resonance; however its entire shape is free in the fit to extract the branching fraction. The PDF for  $\Delta E$  is taken to be a first-order Chebyshev polynomial. The  $m_{\pi^+\pi^-}$  shape is the sum of a second order polynomial, a Breit-Wigner for  $\rho^0$  and a Breit-Wigner for  $f_0(980)$ .  $\mathcal{F}_{S/B}$  is modelled as described before; in addition, we account for a correlation with  $m_{\pi^+\pi^-}$  by multiplying its mean with the factor  $a^l = p_0^l(M_1 + M_2) + 1$ , where  $p_0^l$  is a constant in each  $r$ -bin. The PDF for  $H_1$  and  $H_2$  for continuum and for all other backgrounds are symmetrised 2D histograms. We use sets of several histograms in bins of other fit variables if a treatment of the corresponding correlation is required.

The charm  $B\bar{B}$  background shape is determined from a large sample of MC containing  $b \rightarrow c$  transitions and is further divided into a neutral and a charged  $B$  sample. For both samples,  $\Delta E$  is correlated with the helicity angles and therefore its PDFs in each sample is formed in different bins of  $H_1, H_2$ . We model the neutral component in four areas of  $H_1, H_2$  by first-order Chebyshev polynomials where we also add a Gaussian if  $|H_{1,2}| > 0.65$  or  $|H_{1,2}| > 0.65$  and  $-0.5 < H_{2,1} < 0.65$  (and vice versa),

$$\mathcal{P}_{B^0\bar{B}^0}^{\text{charm}}(\Delta E)_{H_1, H_2} \equiv (fG(\Delta E, \mu, \sigma) + (1 - f)(c_1 C_1(\Delta E)))_{H_1, H_2}, \quad (4)$$

and the charged component with the sum of Chebyshev polynomials up to the third order,

$$\mathcal{P}_{B^\pm B^\mp}^{\text{charm}}(\Delta E)_{H_1, H_2} \equiv \sum_{i=1,2} c_i C_i(\Delta E) + a(H_1, H_2) c_3 C_3(\Delta E). \quad (5)$$

where the cubic term has the factor  $a$  obtained from MC and accounting for the correlation,  $a(H_1, H_2) = b(|H_1| + |H_2|)$  if  $|H_{1,2}| > 0.5$  with a constant  $b = 0.68 \pm 0.01$ . (Otherwise  $a(H_1, H_2) = 1$ ).

The  $m_{\pi^+\pi^-}$  shape of the charm  $B$  decays is described by a first order Chebyshev polynomial where a Gaussian, accounting for  $f_0(600)$ , is added to the neutral decays if  $|H_{k=1,2}| > 0.65$ ,

$$\mathcal{P}_{B^0\bar{B}^0}^{\text{charm}}(m_{\pi^+\pi^-})_{H_1, H_2} \equiv f_{H_1, H_2} c_1 C_1(m_{\pi^+\pi^-})(1 - f_{H_1, H_2}) G(m_{\pi^+\pi^-}, \mu, \sigma). \quad (6)$$

The widths of both Gaussians of the  $\mathcal{F}_{S/B}$  shapes are multiplied with a constant  $d^l$  in the corners of the  $H_1, H_2$  plane,  $|H_{1,2}| > 0.7$  or  $H_{1,2} > 0.5$  and  $H_{2,1} < -0.5$ .

The charmless  $B\bar{B}$  background shape is determined from a large sample of MC events containing  $b \rightarrow u, d, s$  transitions (again, divided into a neutral and a charged category). The  $\Delta E$  distribution of neutral  $B$  decays is described by a Gaussian plus a third-order Chebyshev polynomial, and that of charged  $B$  decays by a first-order Chebyshev polynomial  $\mathcal{P}_{B^\pm B^\mp}^{\text{charmless}} = c_1 C_1(\Delta E)$ , where  $c_1 \equiv p_0 M_1 + p_0 M_2 + p_1(M_1 \times M_2)$  with  $p_0 = -2.44 \pm 0.47$  and  $p_1 = 5.46 \pm 1.08$ . Since the neutral charmless  $M_1, M_2$  distribution is correlated with  $H_1, H_2$ , we describe its shape by the sums of Gaussian and Chebyshev polynomials in five bins of  $H_1, H_2$ , where in most bins also a correlation between the two  $\pi^+\pi^-$  masses is seen. The charged  $m_{\pi^+\pi^-}$  distribution is modeled by a smooth 2D histogram.

The PDF shapes for the remaining four-pion states are determined from individually generated MC samples. For the decay  $B^0 \rightarrow \rho^0 \pi^+ \pi^-$ , we assume a phase space distribution and account for this assumption in the systematic uncertainty. Since we include mis-reconstructed events in the model, a polynomial is added to their  $\Delta E$  PDFs. For the non-resonant decay, the correlation with the helicity angles is incorporated by taking a different width of the core Gaussian for the center of the  $H_1$ - $H_2$  plane. The  $M_1, M_2$  shapes are

TABLE IV: List of peaking backgrounds, assumed branching fractions and their expected yields for SVD1 and SVD2.

Mode	$\mathcal{B} (\times 10^{-6})$	SVD1	SVD2
$B^0 \rightarrow a_1^\pm [\pi^\pm \pi^\mp \pi^\pm] \pi^\mp$	$16.5 \pm 2.5$	65	299
$B^0 \rightarrow a_2^\pm [\pi^\pm \pi^\mp \pi^\pm] \pi^\mp$	$1.65 \pm 1.65$	1	7
$B^0 \rightarrow b_1^\pm [\pi^\pm \pi^\mp \pi^\pm] \pi^\mp$	$0.17 \pm 1.53$	1	3

TABLE V: Summary of yields fixed relative to other yields free in the fit. The mis-reconstructed yield is fixed relative to the signal yield, and the charmed and charmless  $B^+ B^-$  background yields are fixed relative to their respective  $B^0 \bar{B}^0$  background yields. The central values are obtained from MC; the errors are statistically.

Yield	SVD1	SVD2
$N_{\text{Mis}}^s$	$(0.09 \pm 0.0006) N_{\text{Sig}}^{\text{SVD1}}$	$(0.09 \pm 0.0006) N_{\text{Sig}}^{\text{SVD2}}$
$N_{B^+ B^-}^{\text{charm},s}$	$(1.40 \pm 0.07) N_{B^0 \bar{B}^0}^{\text{charm},\text{SVD1}}$	$(1.42 \pm 0.04) N_{B^0 \bar{B}^0}^{\text{charm},\text{SVD2}}$
$N_{B^+ B^-}^{\text{charmless},s}$	$(0.83 \pm 0.08) N_{B^0 \bar{B}^0}^{\text{charmless},\text{SVD1}}$	$(0.86 \pm 0.04) N_{B^0 \bar{B}^0}^{\text{charmless},\text{SVD2}}$

modeled by 2D histograms, except for  $B^0 \rightarrow f_0 f_0$  and  $B^0 \rightarrow f_0 \rho^0$ , where products of two Breit-Wigners are used. Since, for  $B^0 \rightarrow f_0 \rho^0$ , one  $\rho^0$  candidate is a  $\rho^0$  and the other a  $f_0$ , the correlation between  $M_1$  and  $M_2$  is taken into account. The mean of the Gaussian of the  $a_1 \pi$   $\mathcal{F}_{S/B}$  shape is multiplied with  $a = 1 + p_1(M_1 + M_2)$ , to account for the correlation with the masses.

Besides the dominant four-pion contribution  $B^0 \rightarrow a_1^\pm \pi^\mp$ , we also fix the other quasi-two-body  $B$  decay modes in which one of the decay product is a single pion as listed in Table IV, where we assume the unknown branching fraction of  $B^0 \rightarrow a_2^\pm \pi^\mp$  to be 10% of  $B^0 \rightarrow a_1^\pm \pi^\mp$ 's. A recent measurement by Belle supports this assumption [13]. The other two assumed branching fractions are taken from the current world average in Ref. [28].

The total likelihood for 116081  $B^0 \rightarrow \rho^0 \rho^0$  candidate events in the fit region is

$$\mathcal{L} \equiv \prod_{l,s} \frac{e^{-\sum_j N_j^s \sum_{i,s} f_j^{l,s}} N_{l,s}}{N_{l,s}!} \prod_{i=1} \sum_j N_j^s f_j^{l,s} \mathcal{P}_j^{l,s}(\Delta E^i, \mathcal{F}_{S/B}^i, M_1, M_2, H_1, H_2), \quad (7)$$

which runs over event  $i$ , component  $j$ ,  $r$ -bin  $l$  and SVD configuration  $s$ . Instead of two free signal yields  $N_{\text{Sig}}^s$  for each detector configuration, branching fractions for the free four pion final states ( $j$ ) are chosen as single free parameters and incorporated into the fit with

$$N_j^s = \mathcal{B}(B^0 \rightarrow f) N_{B\bar{B}}^s \epsilon_j^s \eta_j^s, \quad (8)$$

where  $\epsilon_j^s$  and  $\eta_j^s$  are given in Tables II and III, respectively. The fraction of events in each  $r$ -bin  $l$ , for component  $j$ , is denoted by  $f_j^{l,s}$ . The fractions of all  $B\bar{B}$  components,  $f_{B\bar{B}}^{l,s}$ , have been calibrated with the  $B^0 \rightarrow D^- [K^+ \pi^- \pi^-] \pi^+$  control sample. In the fit to data, we also float  $f_L$ , the yields  $N_{q\bar{q}}^s$ ,  $N_{B^0 \bar{B}^0}^{\text{charm},s}$  and  $N_{B^0 \bar{B}^0}^{\text{charmless},s}$  and the parameters of the shape of the continuum model. The remaining yields are fixed to the values given in Table V as determined from MC.

## V. FIT RESULT

We perform a six dimensional fit to the data. The projection of the fit results onto  $\Delta E$ ,  $M_1$ ,  $M_2$ ,  $H_1$ ,  $H_2$  and  $\mathcal{F}_{S/B}$  are shown in Fig. 4. The obtained branching fractions, their corresponding yield, upper limits at 90% confidence level are given in Table VI, together with  $f_L$  of  $B^0 \rightarrow \rho^0 \rho^0$ . The statistical correlation coefficients between the observables are given in Table VII.

TABLE VI: Branching fractions with their corresponding yield, upper limits at 90% confidence level and the significances ( $\mathcal{S}$ ) for modes with a positive yield from the fit to data. Furthermore, the longitudinal polarization fraction  $f_L$  of  $B^0 \rightarrow \rho^0 \rho^0$  is given. The errors are statistical and systematic, respectively, statistical errors are given at the  $1\sigma$  level.

Branching fraction ( $\times 10^{-6}$ )	Events	UL ( $\times 10^{-6}$ )	$\mathcal{S}$ ( $\sigma$ )
$\mathcal{B}(B^0 \rightarrow \rho^0 \rho^0) = 1.02 \pm 0.30 \pm 0.22$	166	$< 1.5$	2.9
$f_L = 0.21^{+0.18}_{-0.22} \pm 0.11$	-	-	-
$\mathcal{B}(B^0 \rightarrow \pi^+ \pi^- \pi^+ \pi^-) = -3.58^{+7.75}_{-7.19} \pm 2.99$	-25	$< 11.7$	-
$\mathcal{B}(B^0 \rightarrow \rho^0 \pi^+ \pi^-) = 1.70^{+4.21}_{-4.12} \pm 5.30$	33	$< 12.2$	$< 1$
$\mathcal{B}(B^0 \rightarrow f_0 \pi^+ \pi^-) \times \mathcal{B}(f_0 \rightarrow \pi^+ \pi^-) = -1.34^{+2.12}_{-1.97} \pm 0.98$	-27	$< 3.1$	-
$\mathcal{B}(B^0 \rightarrow f_0 \rho^0) \times \mathcal{B}(f_0 \rightarrow \pi^+ \pi^-) = 0.86 \pm 0.27 \pm 0.15$	149	-	3.0
$\mathcal{B}(B^0 \rightarrow f_0 f_0) \times \mathcal{B}(f_0 \rightarrow \pi^+ \pi^-)^2 = 0.03^{+0.10}_{-0.09} \pm 0.04$	-5	$< 0.2$	-

TABLE VII: Statistical correlations between the observables.

$\mathcal{B}(B^0 \rightarrow X)$	$\rho^0 \rho^0$	$f_L$	$\pi^+ \pi^- \pi^+ \pi^-$	$\rho^0 \pi^+ \pi^-$	$f_0 \pi^+ \pi^-$	$f_0 f_0$	$f_0 \rho^0$
$\rho^0 \rho^0$	1	0.45	-0.03	-0.34	0.04	0.02	-0.02
$f_L$		1	0.06	0.00	0.03	0.01	-0.08
$\pi^+ \pi^- \pi^+ \pi^-$			1	-0.35	-0.23	-0.04	0.00
$\rho^0 \pi^+ \pi^-$				1	-0.07	0.02	-0.24
$f_0 \pi^+ \pi^-$					1	-0.36	-0.20
$f_0 f_0$						1	0.07
$f_0 \rho^0$							1

The resulting  $B^0 \rightarrow \rho^0 \rho^0$  branching fraction is quite consistent with the previous Belle analysis [21] and it is also in agreement with the value obtained by the BaBar collaboration [22]. The fraction of longitudinal polarization in  $B^0 \rightarrow \rho^0 \rho^0$  decays is somewhat lower than previously measured (differing from the BaBar result by  $2.1\sigma$ ) and the branching fraction of  $B^0 \rightarrow f_0 \rho^0$  decays is significantly higher than indicated by previous measurements. We discuss these results in the next section. For the modes where an upper limit was obtained, we have improved values for  $B^0 \rightarrow \pi^+ \pi^- \pi^+ \pi^-$  and  $B^0 \rightarrow f_0 \pi^+ \pi^-$  than the current world averages [28].

The relative contributions of the components modeled in this analysis are found to be 0.1%  $B^0 \rightarrow \rho^0 \rho^0$ , 0.1%  $B^0 \rightarrow f_0 \rho^0$ , 92.8% continuum, 6.7%  $B\bar{B}$  background and 0.3% for the remaining four pion final states.

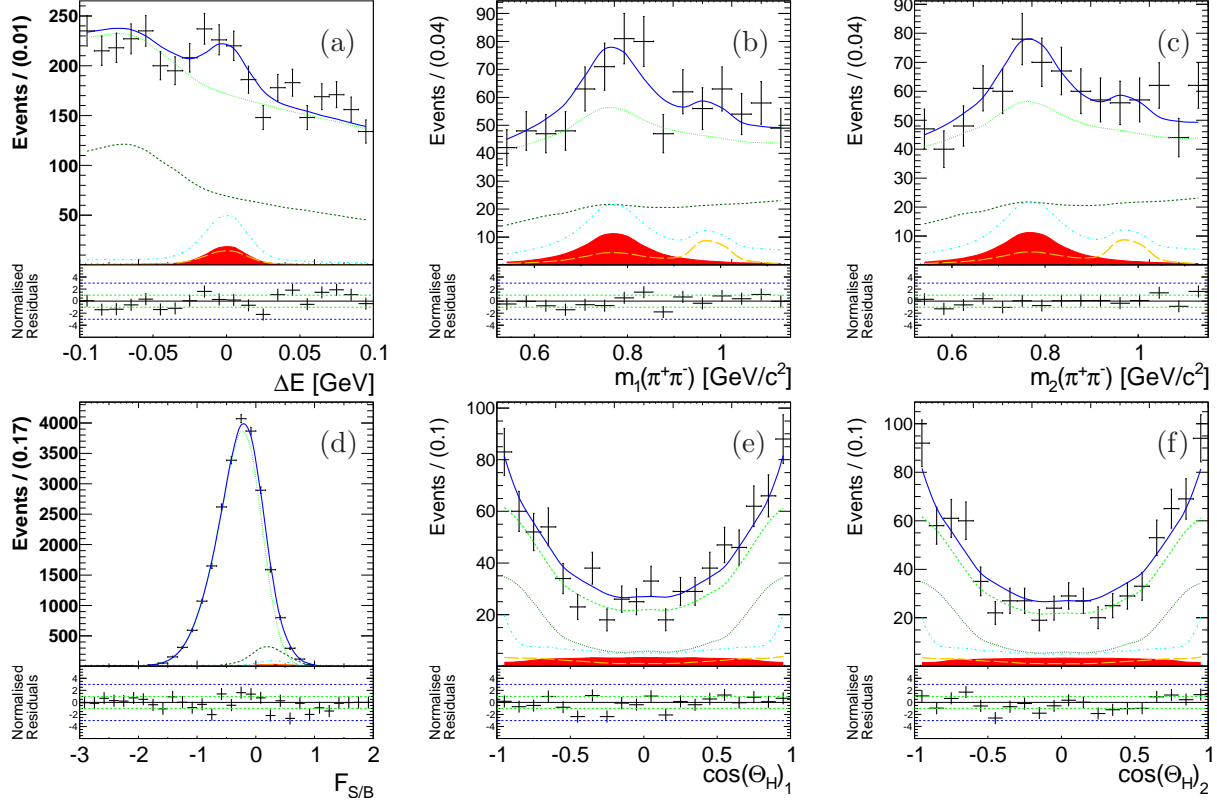


FIG. 4: (color online) Projections of the fit to the data. The points represent the data and the solid curve represents the fit result. The shaded (red) area shows the  $B^0 \rightarrow \rho^0 \rho^0$  and the (orange) long dashed curve the  $B^0 \rightarrow f_0 \rho^0$  contribution. The (cyan) dash-dotted curve shows all four pion final states, the (dark green) dotted curve shows the non-peaking  $B\bar{B}$  contribution and the (bright green) dashed curve shows the total non-peaking background. (a) shows the  $\Delta E$  projection in the  $\mathcal{F}_{S/B} > 0.5$  region. (d) shows the  $\mathcal{F}_{S/B}$  projection in the  $|\Delta E| < 0.02$  GeV region. Here, the dashed curve shows the continuum background contribution. Plots (b,c) and (e,f) show the  $m_{\pi^+\pi^-}$  and  $\cos \theta_H$  projections, respectively, in the  $\mathcal{F}_{S/B} > 0.5$  and  $|\Delta E| < 0.02$  GeV region.



## VI. VALIDITY CHECKS AND SIGNIFICANCE

We investigate the stability of the fit result by removing the components  $B^0 \rightarrow \pi^+\pi^-\pi^+\pi^-$ ,  $f_0\pi^+\pi^-$ , and  $f_0f_0$  from the fit, as for those the nominal fit gives negative yields consistent with zero. The obtained results are given in Table VIII where the fit result remains stable.

TABLE VIII: Fit results from fit to data with the branching fractions of  $B^0 \rightarrow \pi^+\pi^-\pi^+\pi^-$ ,  $f_0\pi^+\pi^-$ , and  $f_0f_0$  are fixed to zero.

Branching fraction ( $\times 10^{-6}$ )	Events
$\mathcal{B}(B^0 \rightarrow \rho^0\rho^0) = 1.05 \pm 0.31$ (stat)	169
$f_L = 0.23 \pm 0.20$ (stat)	—
$\mathcal{B}(B^0 \rightarrow \rho^0\pi^+\pi^-) = -0.32 \pm 3.00$ (stat)	-6
$\mathcal{B}(B^0 \rightarrow f_0\rho^0) \times \mathcal{B}(f_0 \rightarrow \pi^+\pi^-) = 0.76 \pm 0.28$ (stat)	132

We repeat the fit while also fixing the  $B^0 \rightarrow \rho^0\pi^+\pi^-$  yield to zero; this fit result is shown in Table IX. Again, the result is in very good agreement with the nominal fit.

TABLE IX: Fit results from fit to data with the branching fractions of  $B^0 \rightarrow \pi^+\pi^-\pi^+\pi^-$ ,  $f_0\pi^+\pi^-$ ,  $f_0f_0$  and  $\rho^0\pi^+\pi^-$  are fixed to zero.

Branching fraction ( $\times 10^{-6}$ )	Events
$\mathcal{B}(B^0 \rightarrow \rho^0\rho^0) = 1.05 \pm 0.28$ (stat)	169
$f_L = 0.23 \pm 0.19$ (stat)	—
$\mathcal{B}(B^0 \rightarrow f_0\rho^0) \times \mathcal{B}(f_0 \rightarrow \pi^+\pi^-) = 0.76 \pm 0.25$	132

Since the branching fraction of  $B^0 \rightarrow f_0\rho^0$  is larger than indicated by the previous measurement, we investigate the impact on  $B^0 \rightarrow \rho^0\rho^0$  when setting  $\mathcal{B}(B^0 \rightarrow f_0\rho^0) = 0$  and vice versa. We obtain consistent results, given in Table X; in order to visualize each mode separately, the nominal fit projections into the  $\rho^0\rho^0$  and  $\rho^0f_0$  windows are shown in Fig. 5.

TABLE X: Fit results from fit to data with the branching fraction of  $B^0 \rightarrow f_0\rho^0$  or  $B^0 \rightarrow \rho^0\rho^0$  fixed to zero.

Branching fraction ( $\times 10^{-6}$ )	Events
$\mathcal{B}(B^0 \rightarrow \rho^0\rho^0) _{f_0\rho^0=0} = 1.01 \pm 0.31$ (stat)	162
$f_L _{f_0\rho^0=0} = 0.26 \pm 0.21$ (stat)	—
$\mathcal{B}(B^0 \rightarrow f_0\rho^0) _{\rho^0\rho^0=0} = 0.73 \pm 0.21$ (stat)	127

Also, to measure the potential impact of the choice of the starting parameters, we perform an additional likelihood scan with random guesses of the initial parameters, where all fits converge to the same result.

Next we refit the data while fixing  $f_L$  to either 0 or 1. We obtain  $\mathcal{B}(B^0 \rightarrow \rho^0\rho^0)_{f_L=0} = (0.79 \pm 0.22) \times 10^{-6}$  and  $\mathcal{B}(B^0 \rightarrow \rho^0\rho^0)_{f_L=1} = (0.22 \pm 0.24) \times 10^{-6}$ , respectively, which are in agreement with our baseline fit result.

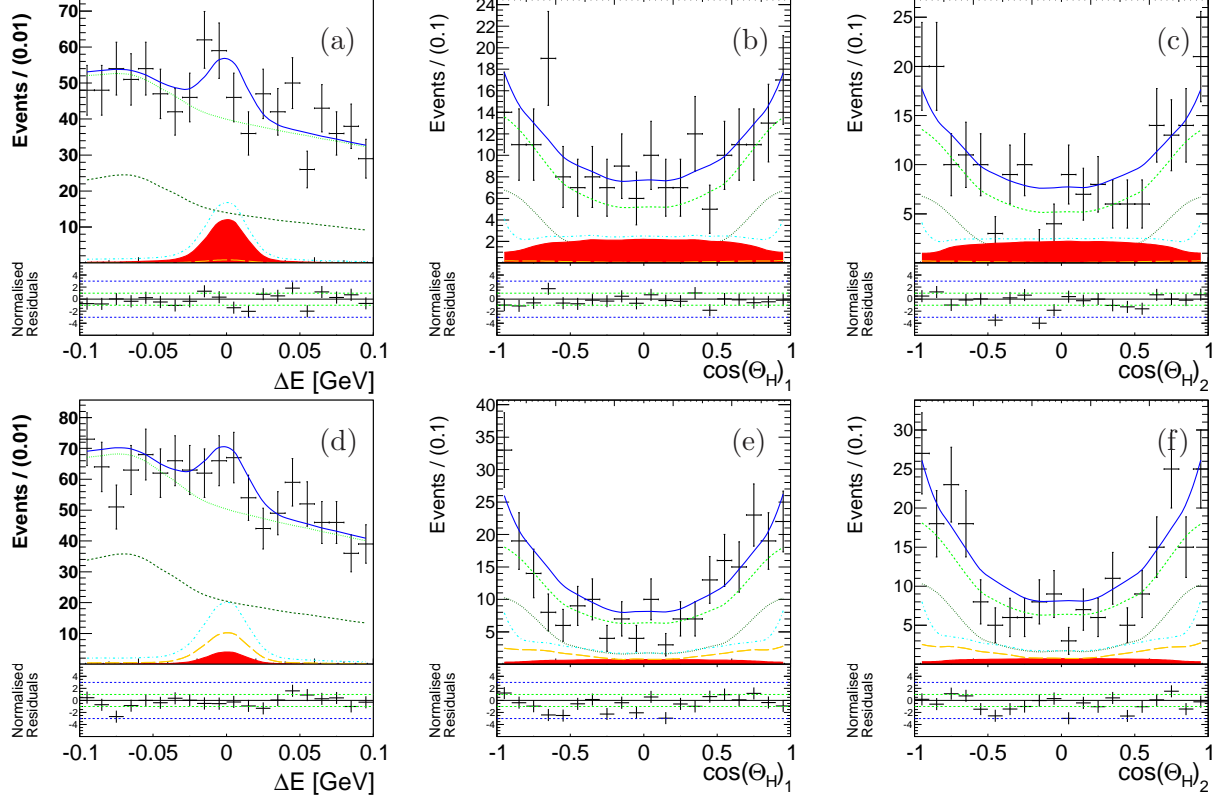


FIG. 5: (color online) In order to better visualize each mode separately, projections of the fit to the data into a  $\rho^0\rho^0$  window  $0.6 \text{ GeV}/c^2 < m_{\pi^+\pi^-} < 0.88 \text{ GeV}/c^2$  (upper row) and a  $f_0\rho^0$  window  $0.6 \text{ GeV}/c^2 < M_{1,2} < 0.88 \text{ GeV}/c^2$  and  $0.88 \text{ GeV}/c^2 < M_{2,1} < 1.08 \text{ GeV}/c^2$  (lower row). The points represent the data and the solid curve represents the fit result. The shaded (red) area shows the  $B^0 \rightarrow \rho^0\rho^0$  and the (orange) long dashed curve the  $B^0 \rightarrow f_0\rho^0$  contribution. The (cyan) dash-dotted curve shows all four pion final states, the (dark green) dotted curve shows the non-peaking  $B\bar{B}$  contribution and the (bright green) dashed curve shows the total non-peaking background. Plots (a) and (d) show the projection into  $\Delta E$  for  $\mathcal{F}_{S/B} > 0.5$  and (b,c) and (e,f) show into  $\cos\theta_H$  for  $\mathcal{F}_{S/B} > 0.5$  and  $|\Delta E| < 0.02 \text{ GeV}$ .

We evaluate the statistical significance  $\mathcal{S}_0$  of the result by taking the ratio of the likelihood of the nominal fit ( $\mathcal{L}_{\text{max}}$ ) and of the fit with the signal yield fixed to zero ( $\mathcal{L}_0$ );

$$\mathcal{S}_0 = \sqrt{-2 \ln \left( \frac{\mathcal{L}_0}{\mathcal{L}_{\text{max}}} \right)}. \quad (9)$$

The statistical significances of the  $B^0 \rightarrow \rho^0\rho^0$  and  $B^0 \rightarrow f_0\rho^0$  yields are found to be  $4.6\sigma$  and  $3.6\sigma$ , respectively. In addition, we demonstrate that the minimum is global by performing likelihood scans of all measured four pion final states as well as  $f_L$ . Likelihood scans of  $B^0 \rightarrow \rho^0\rho^0$ ,  $f_L$  and  $B^0 \rightarrow f_0\rho^0$ , convolved with the corresponding systematic uncertainties, are shown in Fig. 6, and are used to obtain the total significance of these two modes, which are  $2.9\sigma$  and  $3.0\sigma$  respectively, including all systematic uncertainties.

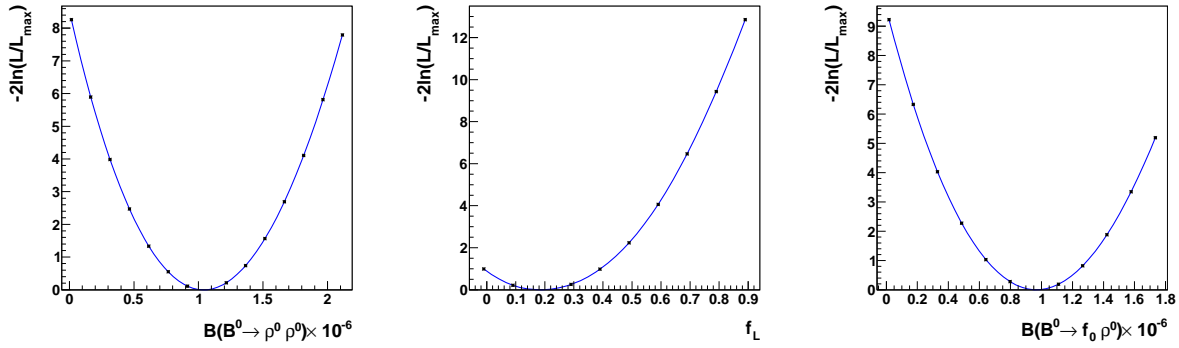


FIG. 6: Likelihood scan of  $\mathcal{B}(B^0 \rightarrow \rho^0 \rho^0)$ ,  $f_L$  and  $\mathcal{B}(B^0 \rightarrow f_0 \rho^0)$  convolved with the systematic uncertainty.

## VII. SYSTEMATIC UNCERTAINTIES

Systematic errors from various sources are considered and estimated with independent internal studies and cross-checks. These are summarized in Table XI. This includes the uncertainty on the number of produced  $B\bar{B}$  events in the data sample. Contributions to the uncertainty in the selection efficiency due to particle identification and tracking are determined by independent studies at Belle.

The uncertainty in the  $\rho^0$  shape is determined by varying the fixed mass within its world average uncertainty [28]. We account for a difference in the fraction of mis-reconstructed events between data and MC by varying this parameter by 5% and repeating the fit. Variations in the parametric model shape due to limited statistics are accounted for by varying each parameter within their errors. Uncertainties in the non-parametric shapes are obtained by varying the contents of the histogram bins within  $\pm 1\sigma$ . The systematic uncertainty due to fixing the peaking background yields of  $B^0 \rightarrow a_1^\pm \pi^\mp$  and  $B^0 \rightarrow b_1^\pm \pi^\mp$  are estimated by varying the branching fraction by its world average error and repeating the fit. For  $B^0 \rightarrow a_2^\pm \pi^\mp$ , where only an upper limit is known, the variation is taken as half of the upper limit. The fit bias was determined from pseudo-experiments by searching for a difference between the generated and fitted physics parameters. For the mode  $B^0 \rightarrow f_0 \rho^0$  we find a non-negligible bias of +16% which is accounted for by subtracting 8% from the fit result and assigning an 8% uncertainty. All other biases are found to be small compared to the statistical uncertainty and are therefore treated fully as systematic uncertainties. Furthermore, we performed an ensemble test where we replaced  $B^0 \rightarrow \rho^0 \pi^+ \pi^-$  helicity PDF with one where the  $\rho^0$  is either longitudinally or transversely polarized to generated MC sets according to the fit result. Modes in agreement with zero events, except  $B^0 \rightarrow \rho^0 \pi^+ \pi^-$ , were not generated, but left free in the fits. The maximal deviation from the nominal model is taken as the uncertainty related to the assumption of the  $B^0 \rightarrow \rho^0 \pi^+ \pi^-$  helicity dependency. Finally, the uncertainty from neglecting interference between the four pion final states was estimated by constructing a 4-body amplitude including detector effects and generating three relative interference configurations between two of the four pion final states: maximum constructive interference, no interference and maximal destructive interference. We consider the modes  $B^0 \rightarrow \rho^0 \rho^0, a_1 \pi, f_0 \rho^0$  and  $\rho^0 \pi \pi$  where for  $\rho^0 \rho^0$  we set  $f_L = 0.21$  and generate MC sets for each combination. For each mode, the largest deviation from the sample with no interference

TABLE XI: Systematic uncertainties of the branching fraction of  $B^0 \rightarrow \rho^0 \rho^0$  and  $f_L$ .

Category	$\delta\mathcal{B}(B^0 \rightarrow \rho^0 \rho^0)$ (%)	$\delta f_L$
$N(B\bar{B})$	1.4	—
Tracking	1.4	—
Particle identification	2.5	—
Mis-reconstruction fraction	1.3	$< 0.001$
$\rho^0$ shape	0.2	$< 0.001$
Model shape	5.1	0.08
Histogram shape	5.2	0.03
$\mathcal{B}(B^0 \rightarrow a_1\pi)$	0.4	0.03
$\mathcal{B}(B^0 \rightarrow b_1\pi)$	$< 0.1$	$< 0.001$
$\mathcal{B}(B^0 \rightarrow a_2\pi)$	$< 0.1$	$< 0.001$
Fit bias	1.9	0.03
Interference	19.2	0.03
$\rho^0\pi\pi$ helicity	6.3	0.05
Total	22.0	0.11

when fitting all sets with a fitter that assumes incoherent decays, gives the systematic uncertainty from interference. We found that interference with  $a_1\pi$  gives the largest uncertainty in all cases.

TABLE XII: Systematic uncertainties (%) for the peaking background modes.

Category	$4\pi$	$\rho^0\pi^+\pi^-$	$f_0\pi^+\pi^-$	$f_0f_0$	$f_0\rho^0$
$N(B\bar{B})$	1.4	1.4	1.4	1.4	1.4
Tracking	1.4	1.4	1.4	1.4	1.4
PID	2.5	2.5	2.5	2.5	2.5
Fit bias	19	10	7	100	8.5
Model shape	28.5	218.8	13.5	13.8	6.5
Histogram shape	38.1	127.3	54.5	46.1	5.9
$\mathcal{B}(B^0 \rightarrow a_1\pi)$	10.3	129.5	3.1	4.7	3.4
$\mathcal{B}(B^0 \rightarrow b_1\pi)$	$< 1$	1.6	$< 1$	$< 1$	$< 1$
$\mathcal{B}(B^0 \rightarrow a_2\pi)$	$< 1$	2.7	$< 1$	$< 1$	$< 1$
Interference	—	93.16	—	—	6.43
$\rho^0\pi\pi$ helicity	26.8	23.3	17.6	14.1	4.5
Total	83.5	312.3	73.07	116.9	15.9

### VIII. $\phi_2$ CONSTRAINT

We use the longitudinally polarized fraction of our result  $\mathcal{B}(B^0 \rightarrow \rho^0 \rho^0)|_{f_L=1} = (0.21 \pm 0.36) \times 10^{-6}$  to obtain a new constraint on the CKM angle  $\phi_2$  through an isospin analysis [16]. For the remaining sides of the triangle we use the current world averages from the Heavy Flavor Averaging Group, Ref. [30]; the longitudinally polarized fraction of  $\mathcal{B}(B^0 \rightarrow \rho^+ \rho^-) = (2.42 \pm 0.31) \times 10^{-5}$  with  $f_L^{+-} = 0.978^{+0.025}_{-0.022}$ ,  $\mathcal{A}_{CP}^{+-} = 0.06 \pm 0.13$ ,  $\mathcal{S}_{CP}^{+-} = -0.05 \pm 0.17$  and  $\mathcal{B}(B^\pm \rightarrow \rho^\pm \rho^0) = (2.4 \pm 0.2) \times 10^{-5}$ . The  $CP$  asymmetries of  $B^0 \rightarrow \rho^0 \rho^0$  are taken from the BaBar measurement [12];  $\mathcal{A}_{CP}^{00} = -0.2 \pm 0.85$ ,  $\mathcal{S}_{CP}^{00} = 0.3 \pm 0.73$ . Fig. 7 shows a probability scan of  $\phi_2$  that is consistent with the SM in its one  $\sigma$  interval of  $\phi_2 = (91.0 \pm 7.2)^\circ$ . The size of the penguin contributions are negligible:  $\Delta\phi_2 = (0.0 \pm 5.4)^\circ$ .

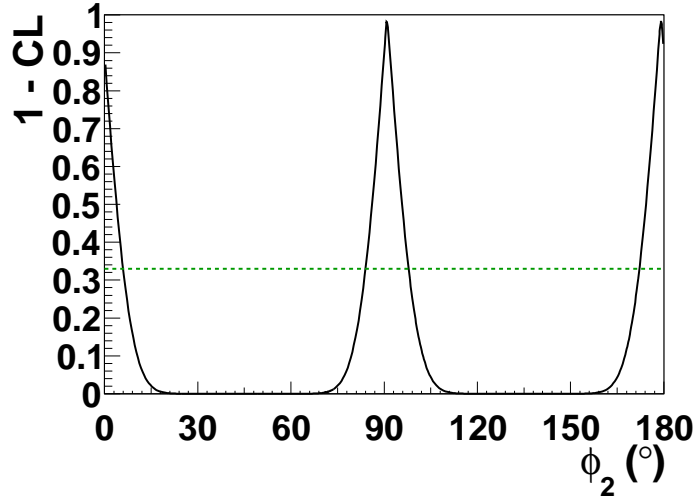


FIG. 7:  $1-\text{CL}$  vs.  $\phi_2$  obtained from an isospin analysis from  $B \rightarrow \rho\rho$  decays. The horizontal line shows the 66% CL.

### IX. CONCLUSION

We have presented a measurement of the branching fraction of  $B^0 \rightarrow \rho^0 \rho^0$  decays and the fraction of longitudinally polarized  $\rho$  mesons in this decay, together with the other four pion final states  $B^0 \rightarrow \rho^0 \pi^+ \pi^-$ ,  $B^0 \rightarrow f_0 \rho^0$ ,  $B^0 \rightarrow f_0 f_0$ ,  $B^0 \rightarrow f_0 \pi^+ \pi^-$  and  $B^0 \rightarrow \pi^+ \pi^- \pi^+ \pi^-$  using the final Belle data set of  $772 \times 10^6 \times B\bar{B}$  pairs. All results are listed in Table VI, where we have upper limits except for  $B^0 \rightarrow f_0 \rho^0$ . There, we report the first evidence with a significance of 3.0 standard deviations. We used the result of longitudinally polarized  $\rho$  mesons in  $B^0 \rightarrow \rho^0 \rho^0$  decays to further constrain the CKM angle  $\phi_2 = (91.0 \pm 7.2)^\circ$  with an isospin analysis. This measurement is still statistically limited and more insight on the interesting and complex structure of four pion final state  $B$  decays will be accessible by future experiments, e.g, by performing a four-body Dalitz analysis.

## Acknowledgments

We thank the KEKB group for the excellent operation of the accelerator, the KEK cryogenics group for the efficient operation of the solenoid, and the KEK computer group and the National Institute of Informatics for valuable computing and SINET4 network support. We acknowledge support from the Ministry of Education, Culture, Sports, Science, and Technology (MEXT) of Japan, the Japan Society for the Promotion of Science (JSPS), and the Tau-Lepton Physics Research Center of Nagoya University; the Australian Research Council and the Australian Department of Industry, Innovation, Science and Research; the National Natural Science Foundation of China under contract No. 10575109, 10775142, 10875115 and 10825524; the Ministry of Education, Youth and Sports of the Czech Republic under contract No. LA10033 and MSM0021620859; the Department of Science and Technology of India; the Istituto Nazionale di Fisica Nucleare of Italy; the BK21 and WCU program of the Ministry Education Science and Technology, National Research Foundation of Korea, and NSDC of the Korea Institute of Science and Technology Information; the Polish Ministry of Science and Higher Education; the Ministry of Education and Science of the Russian Federation and the Russian Federal Agency for Atomic Energy; the Slovenian Research Agency; the Swiss National Science Foundation; the National Science Council and the Ministry of Education of Taiwan; and the U.S. Department of Energy and the National Science Foundation. This work is supported by a Grant-in-Aid from MEXT for Science Research in a Priority Area (“New Development of Flavor Physics”), and from JSPS for Creative Scientific Research (“Evolution of Tau-lepton Physics”).



- 
- [1] N. Cabibbo, Phys. Rev. Lett. **10**, 531 (1963).
  - [2] M. Kobayashi and T. Maskawa, Prog. Theor. Phys. **49**, 652 (1973).
  - [3] K. Abe *et al.* (Belle Collaboration), Phys. Rev. Lett. **87**, 091802 (2001).
  - [4] I. Adachi *et al.* (Belle Collaboration), Phys. Rev. Lett. **108**, 171802 (2012).
  - [5] B. Aubert *et al.* (BaBar Collaboration), Phys. Rev. Lett. **87**, 091801 (2001).
  - [6] B. Aubert *et al.* (BaBar Collaboration), Phys. Rev. D **79**, 072009 (2009).
  - [7] H. Ishino *et al.* (Belle Collaboration), Phys. Rev. Lett **98**, 211801 (2007).
  - [8] B. Aubert *et al.* (BaBar Collaboration), arXiv:0807.4226 (2008).
  - [9] A. Kusaka *et al.* (Belle Collaboration), Phys. Rev. Lett **98**, 221602 (2007).
  - [10] B. Aubert *et al.* (BaBar Collaboration), Phys. Rev. D **76**, 012004 (2007).
  - [11] A. Somov *et al.* (Belle Collaboration), Phys. Rev. D **76**, 011104 (2007).
  - [12] B. Aubert *et al.* (BaBar Collaboration), Phys. Rev. D **76**, 052007 (2007).
  - [13] J. Dalseno *et al.* (Belle Collaboration), arXiv:1205.5957.
  - [14] B. Aubert *et al.* (BaBar Collaboration), Phys. Rev. Lett. **97**, 051802 (2006).
  - [15] B. Aubert *et al.* (BaBar Collaboration), Phys. Rev. Lett. **98**, 181803 (2007).
  - [16] M. Gronau and D. London, Phys. Rev. Lett **65**, 3381 (1990).
  - [17] M. Gronau and J. Zupan, Phys. Rev. D **73**, 057502 (2006).
  - [18] H. Li and S. Mishima, Phys. Rev. D **73**, 114014 (2006).
  - [19] M. Beneke, J. Rohrer and D. Yang, Nucl. Phys. B **Vol. 774**, pages 64-101, (2007).
  - [20] W. Zou and Z. Xiao, Phys. Rev. D **72**, 094026 (2005).
  - [21] C. Chiang *et al.* (Belle Collaboration), Phys. Rev. D **78**, 111102 (2008).
  - [22] B. Aubert *et al.* (BaBar Collaboration), Phys. Rev. D **78**, 071104 (2008).
  - [23] S. Kurokawa and E. Kikutani, Nucl. Instr. and Meth. A **499**, 1 (2003), and other papers included in this volume.
  - [24] A. Abashian *et al.* (Belle Collaboration), Nucl. Instr. and Meth. A **479**, 117 (2002).
  - [25] Z. Natkaniec *et al.* (Belle SVD2 Group), Nucl. Instr. and Meth. A **560**, 1 (2006).
  - [26] R. Brun *et al.*, GEANT 3.21, CERN DD/EE/84-1 (1984).
  - [27] H. Tajima *et al.*, Nucl. Instr. and Meth. A **533**, 370 (2004).
  - [28] J. Beringer *et al.* (Particle Data Group), Phys. Rev. D **86**, 010001 (2012)
  - [29] H. Kakuno *et al.*, Nucl. Instr. and Meth. A **533**, 516 (2004).
  - [30] Y. Amhis *et al.*, Heavy Flavor Averaging Group (HFAG), Averages of b-hadron, c-hadron, and  $\tau$ -lepton properties as of early 2012, arXiv:hep-ph/1207.1158.